Control of Mechanical Behavior in Polyolefin Composites: Integration of Glassy, Rubbery, and Semicrystalline Components

Mahesh K. Mahanthappa,[†,‡] Lisa S. Lim,[†] Marc A. Hillmyer,[‡] and Frank S. Bates*[,†]

Department of Chemical Engineering and Materials Science and Department of Chemistry, University of Minnesota, Minneapolis, Minnesota 55455

Received August 1, 2006; Revised Manuscript Received November 17, 2006

ABSTRACT: The mechanical properties of a homologous series of polyolefin block copolymers comprised of glassy poly(cyclohexylethylene) (C), elastomeric poly(ethylene-*alt*-propylene) (P), and semicrystalline poly(ethylene) (E) are documented. Monodisperse CPEPC, CPE, and CEPEC with mass fractions $w_C \sim 0.39-0.44$ and $0 \leq \xi \leq 1$, where $\xi = w_E/(w_E + w_P)$, were synthesized by sequential anionic polymerization of styrene, isoprene, and butadiene followed by catalytic hydrogenation. These materials hierarchically microphase separate into lamellae, within which templated crystallization-induced segregation occurs. As ξ increases, the unoriented, polydomain CPEPC materials exhibit monotonically increasing elastic moduli and yield stresses, comparable ultimate tensile strengths, and decreasing failure strains. Cold drawing the CPEPC polymers yields high-strength materials, the structures of which are examined by small- and wide-angle X-ray scattering. Drawn CPEPC-70 ($\xi = 0.70$) exhibits improved toughness with an ultimate tensile strength $\sigma_{fail} = 75 \pm 10$ MPa and elongation at break of $\epsilon_{fail} = 1.22 \pm 0.22$, as compared to $\sigma_{fail} = 92 \pm 21$ MPa and $\epsilon_{fail} = 0.86 \pm 0.18$ for drawn CEC ($\xi = 1.00$). Elasticity measurements on the drawn samples demonstrate that materials with $\xi > 0$ exhibit low degrees of stress softening, while smaller permanent sets and higher failure strains are observed as ξ decreases.

Introduction

Styrenic block copolymer thermoplastic elastomers find ubiquitous application in everyday items including footwear, pressure-sensitive adhesives, asphalt modifiers, and roofing compounds.[1] These block copolymers incorporate the mechanical responses of glassy polystyrene (S) and rubbery poly(butadiene) (B) or poly(isoprene) (I) into a microphase-separated structure, wherein glassy S blocks anchor the ends of the amorphous rubber in linear sequences such as SBS and SIS. Supplemented by small-angle X-ray scattering (SAXS) and transmission electron microscopy (TEM), studies of the mechanical properties of polydomain and "single-grain" lamellae-, cylinder-, and sphere-forming triblock copolymers have established the origins of improved strength in these materials relative to their constituent homopolymers.[2−9] Microdomain structure and orientation coupled with the slippage of trapped entanglements in the rubbery block govern the mechanical properties at small strains (e.g., elastic modulus).[1,10] At large strains, grain rotation and buckling disrupt the microdomain structure, culminating in a mechanical response ultimately controlled by chain deformation and orientation.[2,3,9] In spite of their widespread use, these materials exhibit several practical limitations including a low upper service temperature (UST) specified by the glass transition temperature of polystyrene ($T_g \sim 100$ °C) and chemical instability due to the polydiene blocks.[11]

Exhaustive hydrogenation of polystyrene over a silica-supported Pt/Re catalyst produces poly(cyclohexylethylene) (PCHE or C), an engineering thermoplastic that mitigates some of the shortcomings of its parent polystyrene.[12] While PCHE exhibits a higher UST than S since $T_{g,C} \sim 147$ °C, its large entanglement molecular weight ($M_e \sim 40.2$ kDa) renders PCHE brittle.[13] Catalytic hydrogenation of S/B block copolymers produces microphase-separated materials comprised of PCHE and semicrystalline polyethylene (E), such as CEC or CECEC. These materials possess greatly enhanced toughness compared to C homopolymer.[12] Synthetic manipulation of the vinyl content of the diene block of the unsaturated block copolymer precursor provides a means for varying the degree of crystallinity in the E block,[14] enabling access to an array of materials that span the continuum from plastics to elastomers. Therefore, C/E glassy−semicrystalline block copolymers offer new opportunities in applications that require chemically resistant, oxidatively stable, optically clear materials. The phase behavior, mechanical properties, and processing characteristics of C/E block copolymers have been extensively documented.[11,15−23]

In contrast to the well-studied mechanical properties of block copolymers derived from pairwise incorporation of glassy and either elastomeric[2,4−9] or semicrystalline[17,18,20,21] segments, the properties of block copolymers comprised of glassy, elastomeric, *and* semicrystalline segments are relatively unstudied. Balsamo et al. investigated the properties of S−B−CL (CL = poly(ϵ-caprolactone)), which forms distorted core−shell cylinders of CL coaxially insulated from the S matrix by rubbery B blocks.[24] The improved toughness of S−B−CL as compared to S−CL diblocks[25] implies that the onset of failure is delayed by incorporation of a rubbery segment. Recently, Schmalz et al. interrogated the properties of S−P−E (P = poly(ethylene-*alt*-propylene)) triblock copolymers, in which cylinders of S and crystallites of E are embedded in a rubbery P matrix.[26] The ultimate properties of these materials do not appreciably differ from those of SPS triblocks. Schmalz et al. attribute the inferior elastic recovery of SPE as compared to SPS at high strains to the ease of irreversible plastic deformation of the E blocks. Differences in the chemical incompatibilities of S, P, and E limit the validity of this comparative study, since the allowed chain conformations and microphase-separated structures adopted in the solid state greatly differ for SPE and SPS. As the authors note, the SPE sequence forces the polymer to adopt extended chain conformations due to the incompatibility of the S and E segments, whereas the SPS architecture permits "bridging" and

* To whom correspondence should be addressed. E-mail: bates@cems.umn.edu.
[†] Department of Chemical Engineering and Materials Science.
[‡] Department of Chemistry.

10.1021/ma0617421 CCC: $37.00
Published on Web 02/01/2007

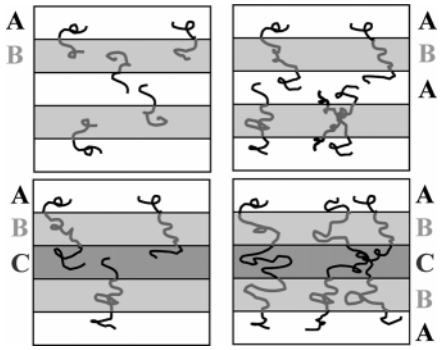

Figure 1. Possible chain conformations for AB, ABA, ABC, and ABCBA block copolymers presenting the analogy between possible chain conformations in ABA and ABCBA.

"looping" chain conformations.

Lamellae-forming block copolymers comprised of glassy, elastomeric, and semicrystalline blocks provide an ideal platform for structure−property investigations aimed at understanding the roles of the constituent blocks in dictating mechanical response. While the mechanical properties of nonlamellar morphologies are dominated by those of the majority (matrix) component, the lamellar structure effectively unmasks the contributions of each block to the overall properties. Appropriate comparisons of the properties of block copolymers comprised of two and three monomers mandate judicious choice of lamellae-forming chain architectures. For AB diblock copolymers, each chain spans only a portion of the period of the lamellar structure, whereas an ABA triblock copolymer chain may span one full lamellar period (see Figure 1). Analogously, an ABC triblock copolymer spans only a portion of the repeating lamellar period, while the palindromic pentablock copolymer ABCBA spans one full lamellar period in the extended chain conformation. Therefore, a comparison of the mechanical properties of two monomer (A and B) and three monomer (A, B, and C) block copolymers having similar chain conformations is best drawn between ABA triblock and ABCBA pentablock copolymers.

Herein, we characterize the morphology and mechanical properties of pentablock copolymers constituted of glassy C, elastomeric P, and semicrystalline E segments. Attention focuses on the properties of five lamellae-forming CPEPC block copolymers having overall C weight fraction $w_C \sim 0.4$, in which weight fractions w_P and w_E are systematically varied at near constant melt segregation strength. Varying w_E results in a series of materials exhibiting remarkable toughness and tunable elastic response. On the basis of our previous report on cold drawing semicrystalline block copolymers to produce high-strength fibers,[22] we examine the effects of cold drawing on the properties of the CPEPC materials. Furthermore, the elastic properties of the drawn materials within the series are compared.

Experimental Section

Block Copolymer Synthesis. Initiated by *sec*-butyllithium at 40 °C in cyclohexane under anaerobic and anhydrous conditions, purified styrene (S), isoprene (I), and butadiene (B) monomers were sequentially anionically polymerized to produce parent SIS, SIB, SIBIS, SBIBS, and SBS block copolymers.[27] An aliquot of the initial styrene block was removed by syringe after 8 h and saved for further analysis (see below), before proceeding with the sequential monomer addition sequence.

The molecular weight distributions of the initial styrene blocks and the final palindromic block copolymers were quantified by size-exclusion chromatography (SEC) at 22 °C in THF (1.0 mL/min flow rate) on a Waters 717 GPC equipped with three Polymer Labs Mixed-C type columns using polystyrene standards. In all cases, the samples yielded monomodal SEC traces with $M_w/M_n \leq 1.1$. The absolute molecular weight of the initial S block was determined using a SEC instrument equipped with three Phenogel (Phenomenex) columns, a refractive index detector, and a Wyatt Optilab DSP light scattering detector. The latter analysis employed a THF mobile phase and the known value $dn/dc = 0.1945$ g/cm^3 for polystyrene in THF at 25 °C.[28]

Quantitative ^{1}H NMR spectra of the unsaturated polymers were recorded in $CDCl_3$ on a Varian UI-500 spectrometer with a 20 s pulse repetition delay to determine the weight fractions of polybutadiene, polyisoprene, and polystyrene. ^{1}H NMR spectra establish that the isoprene polymerizations proceed with predominant 4,1-monomer insertion with ~6 mol % 4,3-insertions. Similarly, butadiene polymerizations display a high degree of 1,4-regioselectivity with ~8 mol % 1,2-insertions.

Catalytic hydrogenation of the unsaturated block copolymers at 170 °C in degassed cyclohexane under 500 psig of H_2 for 12 h using a silica-supported Pt/Re catalyst[12] (Dow Chemical Co.) furnished the desired CPC, CPE, CPEPC, CEPEC, and CEC block copolymers. Polymers were precipitated in MeOH, filtered, and dried in vacuo at 70 °C to a constant weight. The extent of hydrogenation determined by ^{1}H NMR spectroscopy in tetrachloroethane-d_2 at 100 °C is greater than 97%. High-temperature SEC analyses at 140 °C in 1,2,4-trichlorobenzene demonstrate that the fully saturated copolymers exhibit narrow molecular weight distributions, confirming that the hydrogenation reaction does not cause degradation reactions. Assuming complete hydrogenation, M_n and the volume fractions of C, P, and E for each saturated polymer were calculated from composition data for the unsaturated precursor, the absolute molecular weight (M_n) of the initial S block, and bulk homopolymer densities at 140 °C.[29] Based on ^{1}H NMR analyses of the unsaturated precursors, the polyethylene segments contain 21 ethyl branches per 1000 carbon atoms, and the poly(ethylene-*alt*-propylene) segments contain 15 isopropyl branches per 1000 carbon atoms. Detailed characterization information for each polymer is given in Table 1.

Thermal Analysis. Differential scanning calorimetry was performed using a TA Instruments Q1000 DSC. The thermal history of each sample was erased by heating to 150 °C for 10 min before cooling to −80 °C at 5 °C/min. The reported second heating and cooling data were collected at a temperature ramp rate of 5 °C/min from −80 to 150 °C.

Dynamic Mechanical Spectroscopy. Order−disorder phase transition temperatures (T_{ODT}) were determined by dynamic mechanical spectroscopy (DMS) measurements using a Rheometrics Scientific ARES strain-controlled rheometer fitted with 25 mm diameter parallel plates. All measurements were conducted in the linear viscoelastic regime ($|\gamma| = 0.5-1\%$), as determined from dynamic strain sweep measurements conducted at 140 °C. The dynamic elastic storage shear modulus (G') was measured as a function of temperature at a frequency $\omega = 1$ rad/s and a strain $|\gamma| = 1\%$ in isochronal temperature ramp tests, using a heating rate of 2 °C/min and a cooling rate of 5 °C/min. Isothermal frequency sweeps from $100 \leq \omega \leq 0.01$ rad/s with $|\gamma| = 0.5-1\%$ were conducted at several temperatures to confirm the location of T_{ODT}.

WAXS. Two-dimensional wide-angle X-ray scattering (WAXS) data were acquired at room temperature on a Bruker AXS (Siemens) microdiffractometer using a 5.92 cm sample-to-detector distance. Experiments employed Cu Kα X-rays generated from a 4XE short anode, monochromated using flat graphite, and collimated through two 0.8 mm pinholes.

SAXS. Synchrotron small-angle X-ray scattering (SAXS) measurements were performed at the 5IDD beamline of the DuPont-Northwestern-Dow Collaborative Access Team Synchrotron Research Center at the Advanced Photon Source (Argonne, IL). Experiments employed a beam energy of 8 keV ($\lambda = 1.54$ Å) and a 3.026 m sample-to-detector distance. Two-dimensional SAXS patterns were recorded on a MAR-CCD detector (133 mm diameter active circular area) with 2048 × 2048 pixel resolution. Samples were heated to $T_{ODT} + 10$ °C (see Table 1) for 5 min, cooled to

Table 1. Characterization Data for CEC, CPC, and CPEPC Block Copolymers

sample	M_n (kg mol^{-1})	M_w/M_n[a]	w_C	w_P	w_E	N[c]	T_{ODT} (°C)[d]	RPA T_s (°C)[e]	q^* (Å^{-1})[f]	d (nm)	$T_{m,E}$ (°C)[h]	X_c (%)[i]	overall E cryst (%)
CEC	29.8	1.02	0.424	0	0.576	503	217	257	0.0303	20.8	94.2	17.7	10.2
CPEPC-70	30.7	1.15	0.411	0.178	0.411	518	236	229	0.0290	21.6	93.7	24.5	10.1
CPEPC-50	30.9	1.11	0.441	0.281	0.278	519	208	209	0.0314	20.0	92.8	31.6	8.8
CPEPC-30	38.6	1.12	0.394	0.423	0.183	650	237	245	0.0282	22.3	84.5	39.8	7.3
CPC	46.1	(1.03)[b]	0.395	0.605	0	776	234	263	0.0273	22.9			
CPEPC-50b	29.8	(1.03)[b]	0.427	0.283	0.29	500	162	193	0.0340[g]	18.5	91.8	34.5	10.0
CPE-50	16.2	(1.03)[b]	0.412	0.29	0.298	286	168	188	0.0350[g]	17.9	104.5	32.1	9.6
CEPEC-50	33.2	(1.03)[b]	0.424	0.29	0.286	563	<125	225			91.9	27.0	7.7

[a] Determined by size exclusion chromatography (SEC) with PS calibration standards in trichlorobenzene at 135 °C. [b] Measured for the unsaturated precursor by SEC in tetrahydrofuran at 25 °C. [c] Calculated using bulk homopolymer densities reported in ref 29 with the 118 Å^3 reference volume. [d] Measured by dynamic mechanical spectroscopy. [e] Calculated using the random phase approximation as described in ref 41. [f] Measured at 150 °C by synchrotron SAXS. [g] Measured by lab source SAXS at 150 °C. [h] Peak melting temperature of the polyethylene (E) block determined by DSC. [i] Percent crystallinity in the E block.

Table 2. Ultimate Properties of Undrawn CEC, CPC, and CPEPC Block Copolymers

sample	E (MPa)	σ_{yield} (MPa)	ϵ_{fail}	σ_{fail} (MPa)
CPE-50	218 ± 13		0.067 ± 0.045	7.5 ± 3.3
CEC	156 ± 20	18.5 ± 0.8	3.76 ± 1.14	22.4 ± 3.5
CPEPC-70	106 ± 8	16.4 ± 0.4	4.18 ± 0.28	29.8 ± 3.3
CPEPC-50	72 ± 6	11.9 ± 0.5	4.86 ± 0.15	38.0 ± 4.3
CPEPC-30	53 ± 4	10.1 ± 0.4	5.03 ± 0.20	29.3 ± 3.1
CPC	28 ± 4	4.9 ± 0.2	6.52 ± 0.65	29.6 ± 3.3

150 °C at 10 °C/min, and held at 150 °C for 5 min before collecting SAXS patterns (typical exposure times ~20 s). Upon cooling a given sample to 22 °C at 10 °C/min and allowing it to rest for 5 min, a second pattern was taken.

Laboratory source SAXS measurements were performed in the Institute of Technology Characterization Facility at the University of Minnesota. Cu Kα X-rays generated by a Rigaku RI-200VBH rotating anode were collimated using two Max-Flux multilayer confocal mirrors (Osmic, Inc.) followed by three pinhole apertures to reduce the final beam diameter to 0.5 mm. Samples were mounted in a helium-purged sample chamber, and data acquisition employed a Siemens Hi-STAR area detector at a 1.583 m sample-to-detector distance.

Polymer Processing and Tensile Testing. Polymer films were produced by compression-molding between Teflon sheets at $T = T_{ODT} + 10$ °C for 10 min at 13.9 MPa, followed by cooling to room temperature at 10 °C/min. Rectangular tensile bars measuring 15 mm × 2 mm × 1 mm were cut from these films using a fresh razor blade. Uniaxial tensile tests were carried out at 22 °C using a Rheometrics Scientific MINIMAT operating with a crosshead speed of 5 mm/min (length-independent strain rate of 0.010 s^{-1}) with an initial gage length of 8 mm. These force−displacement measurements were converted to engineering stress $\sigma = F/A_0$ vs nominal strain $\epsilon = (l - l_0)/l_0$, where A_0 and l_0 are respective the initial cross-sectional area and length, respectively. The modulus of each sample was determined by linearly fitting the elastic portion of the stress−strain curve before the yield point. All reported data reflect an average over a minimum of five independent trials.

Cold drawn tensile samples were produced by drawing rectangular tensile samples to the completion of necking (ϵ_{neck} in Table 3) at 22 °C using a MINIMAT at a drawing rate of 0.010 s^{-1}. Upon releasing the samples from tension, the tensile bars exhibited the permanent set reported in Table 3. Samples were aged at 22 °C for 24 h before their ultimate properties were tested using a 8 mm gage length on the MINIMAT at a strain rate of 0.010 s^{-1}.

Cyclic tensile−compression tests were executed at 22 °C on the cold-drawn samples using the MINIMAT at a strain rate of 0.010 s^{-1}. Fifteen tensile−compression cycles were performed as follows: a drawn sample was strained to 60% of the average breaking strain (see Table 2) and compressed to its initial 8 mm gage length. Samples were not unloaded from the testing apparatus between cycles, and there was a 1 s delay between cycles.

Results

Phase Behavior and Morphology. The molecular parameters for the multiblock copolymers synthesized in this study are provided in Table 1. Since all polymers have $w_C \sim 0.4$, the primary compositional difference in the series is parametrized by the dimensionless quantity

$$\xi = w_E/(w_E + w_P)$$

We employ the following nomenclature to refer to each polymer sample: the letters specify the block sequence, and the following number indicates the value of 100ξ. (Note that $\xi = 1$ and $\xi = 0$ correspond to CEC and CPC, respectively.) Cold drawn samples are further identified by a "*d*" preceding the block sequence as in *d*CPEPC-50.

The order−disorder transition temperature, T_{ODT}, for each block copolymer was determined by dynamic mechanical spectroscopy (DMS)[30,31] (Table 1). The first-order phase transition from the microphase-separated state to the disordered melt is characterized by an abrupt drop in the dynamic storage modulus G' in isochronal temperature ramp tests. Isothermal frequency sweep data acquired above and below T_{ODT} confirm the location of the order−disorder transition. The observed nonterminal rheological response $G' \sim G'' \sim \omega^{0.5}$ below T_{ODT} (not shown) suggests that these materials adopt a lamellar morphology.[31]

Both molecular weight and linear block sequence influence the phase behavior of pentablock copolymers comprised of C, P, and E. The large difference in T_{ODT} for compositionally similar CPEPC-50 and CPEPC-50b underscores the sensitive dependence of the melt segregation strength on small changes in molecular weight. At similar compositions and molecular weights, comparison of CPEPC-50 and CEPEC-50 illustrates an unexpected consequence of block sequence on polyolefin melt phase behavior. CEPEC-50 is melt-disordered, i.e., $T_{ODT} < T_{g,C} \sim 125$ °C, in sharp contrast to the melt-ordered CPEPC-50 having $T_{ODT} = 208$ °C. The possible origins of these two surprising observations are addressed in the Discussion section.

Each of the CPEPC block copolymers exhibits a synchrotron SAXS pattern consistent with a lamellar microdomain structure at 22 and 150 °C (Figure 2). Diminished intensity of the 3q^* peak is observed in all samples except CEC. The diminished intensity of the 3q^* peak in these SAXS patterns is attributed to the fact that $f_C \sim 0.37$ and the electron densities of the E and P blocks in the melt at 150 °C are very similar. Domain spacings $d \sim 18-23$ nm were calculated from the magnitude of the principal scattering wave vector $|\mathbf{q}^*| = 2\pi/d$ at 150 °C. The negative concavity of the baselines of the azimuthally integrated SAXS patterns acquired at 22 °C (Figure 2a) stems from overlap

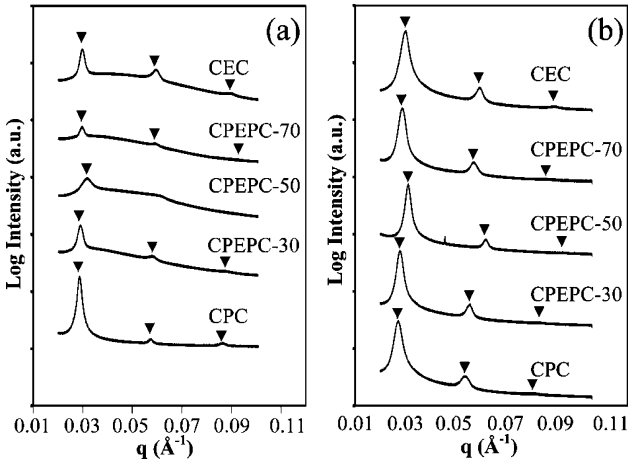

Figure 2. Log intensity vs q ($Å^{-1}$) plots generated from azimuthal integrations of two-dimensional synchrotron SAXS patterns for CPEPC block copolymers at (a) 22 and (b) 150 °C with indexing for a lamellar phase.

of scattering intensity associated with the microphase-separated structure (sharp peaks) and that for the intercrystal spacing of the semicrystalline polyethylene within the microdomains (a single broad peak). The intercrystal spacing in E homopolymer produced by hydrogenation of 1,4-polybutadiene is $d \sim 14$ nm ($q = 0.045$ $Å^{-1}$).[32] Lab source SAXS analyses confirm that CPEPC-50b and CPE-50 also adopt a lamellar morphology in the melt. CEPEC-50 exhibits only correlation-hole scattering associated with melt disorder, consistent with the DMS results. Temperature-dependent SAXS measurements confirm the location of the order−disorder transition temperatures determined by rheology; this first-order phase transition results in dissolution of the higher order scattering peaks to yield correlation-hole scattering.[33]

The thermal properties of the CPEPC polyolefins are also listed in Table 1. The peak melting temperatures of the E blocks in the CEC and CPEPC copolymers are in the range 83−94 °C, as expected for confined crystallization of polyethylene in C-containing block copolymers.[34] The crystallinity, X_c, for each sample was calculated from the heat of melting (ΔH_m) measured by DSC using the expression

$$X_c = \Delta H_m / w_E \Delta H^\circ_{m,E}$$

where ($\Delta H^\circ_{m,E}$) = 277 J/g is the theoretical heat of melting for perfectly crystalline polyethylene.[28] As ξ increases, $T_{m,E}$ increases and X_c linearly decreases such that the overall weight fraction of crystalline material in all E-containing polymers fortuitously remains nearly constant ($w_E X_c \sim 7.3-10.2\%$). The loose E chain end in CPE-50 confers added chain mobility upon the E block, enabling more complete block crystallization. Consequently, CPE-50 exhibits a higher melting temperature than CPEPC-50. This behavior parallels the previously reported higher melting temperature of a CE diblock as compared to a CEC triblock copolymer.[34]

Mechanical Properties of Polydomain Samples. Representative engineering stress (σ) vs nominal strain (ϵ) curves for the C/P/E materials are shown in Figure 3, and the ultimate properties of these materials are compiled in Table 2. The brittleness of CPE-50 (Figure 3 inset) sharply contrasts the toughness of CPEPC-50. The striking difference between this result and the apparent ductility of SPE triblocks[26] probably originates in their different microphase-separated morphologies. Uniaxial extension of the CPEPC samples beyond the yield point results in plastic deformation ("necking" or "cold drawing"),

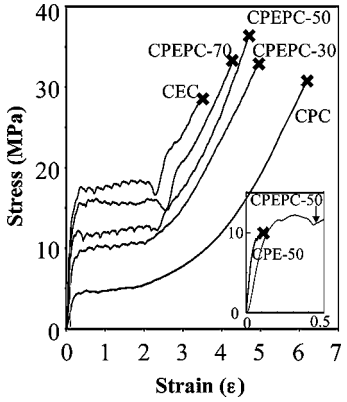

Figure 3. Representative stress vs strain curves for undrawn CPEPC materials. The inset (right) shows the brittle properties of CPE-50 relative to CPEPC-50.

Table 3. Cold Drawing Parameters for CEC, CPC, and CPEPC Block Copolymers

sample	ϵ_{neck}[a]	permanent set[b]
CEC	2.84 ± 0.13	2.05 ± 0.20
CPEPC-70	3.04 ± 0.11	1.83 ± 0.05
CPEPC-50	2.69 ± 0.12	1.33 ± 0.09
CPEPC-30	2.47 ± 0.06	0.68 ± 0.05
CPC	2.34 ± 0.15	0.27 ± 0.04

[a] Strain at the completion of necking. [b] Permanent set was calculated by measuring the final length of the drawn fiber immediately upon release from tension.

followed by strain hardening and ultimate failure. The elastic modulus (E) and the yield stress (σ_{yield}) associated with each CPEPC polymer increase monotonically with ξ, while the elongation at break (ϵ_{fail}) decreases. Since most of the samples fail in close proximity to the grips, the reported values for σ_{fail} represent lower bounds on the ultimate tensile strengths of these materials.

Effects of Cold Drawing. Based on a previous report that cold drawing CEC and CECEC produces high-strength fibers,[22] the effects of cold drawing on the mechanical properties of CPEPC block copolymers were investigated. Cold drawn tensile samples were produced at 22 °C by straining tensile bars to $\epsilon_{neck} \sim 2.5-3$, corresponding to the end of the necking deformation (Table 3). Upon releasing a sample from tension, the gauge length was immediately measured to determine the permanent set. The permanent set increases with increasing ξ, suggesting that the size of the E crystals specifies the magnitude of irreversible plastic deformation (vide infra).

SAXS and WAXS analyses of the drawn samples indicate that cold drawing changes the solid-state morphology of the samples (Figure 4). The polydomain block copolymer samples initially possess a random orientation of the lamellar grains and the E crystallites within the microdomains, as inferred from the isotropic 2D SAXS and WAXS patterns, respectively. Deformation of the lamellar grains by cold drawing yields an elliptical SAXS pattern analogous to that documented for *d*CEC and *d*CECEC.[22] The scattering intensity along the contour of the ellipse is nonuniform for all materials, with a notable reduction in intensity along the draw direction. The eccentricity of the ellipse formed by *d*CPEPC materials increases with ξ, with an attendant increase in permanent set (Figure 4). The SAXS pattern of *d*CPEPC-50 exhibits four bright scattering peaks ±23° from the equator at the same $|\mathbf{q}|$ as the isotropic ring of the undrawn sample, suggesting a preferred lamellar orientation without a change in the domain spacing (Figure 5a,c). WAXS analysis indicates the alignment of the E crystallites such that

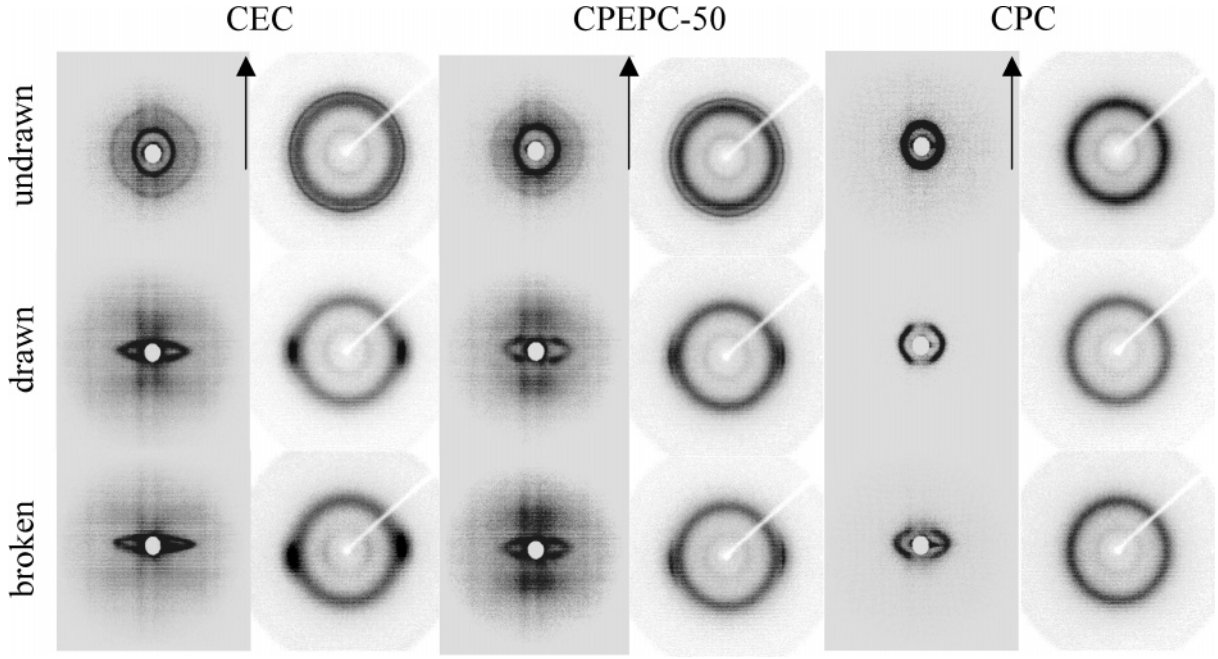

Figure 4. Lab source 2D SAXS and WAXS patterns of undrawn (polydomain), drawn, and released from tension and broken CEC, CPEPC-50, and CPC. Arrows indicate the drawing direction.

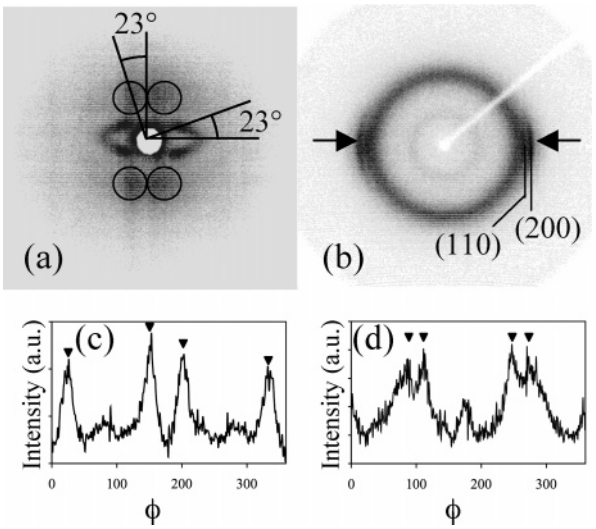

Figure 5. (a) A 2D SAXS pattern of drawn CPEPC-50 exhibiting four intense spots ±23° ($q = 0.031$ Å^{-1}) from the equator and four diffuse spots located at ±23° ($q = 0.043$ Å^{-1}) from the meridian. (The drawing axis coincides with the vertical direction.) (b) WAXS pattern of drawn CPEPC-50 noting the (110) and (200) reflections; (c) and (d) azimuthal integrations of the 2D SAXS pattern in (a) with 0.026 Å^{-1} ≤ q ≤ 0.035 Å^{-1} and 0.046 Å^{-1} ≤ q ≤ 0.058 Å^{-1}, respectively.

the molecular axes of the polyethylene chains coincide with the drawing direction (Figure 4). This last observation echoes similar results for cold drawn E-containing multiblock copolymers[22,35] and melt-spun high-density polyethylene.[36] The oriented E crystals produce two pairs of broad scattering maxima at $q = 0.043$ Å^{-1} above and below the ellipse observed by SAXS, implying an unperturbed intercrystal spacing $d \sim 14$ nm within the E domains (Figures 4 and 5a). These SAXS scattering maxima are located ±23° from the meridian in *d*CPEPC-50 (Figure 5d). The drawn CPC sample exhibits a low degree of permanent set consonant with a smaller eccentricity of the elliptical SAXS pattern. WAXS patterns of the drawn CPC show no apparent preferential alignment of the amorphous P chains.

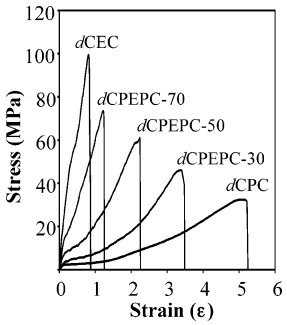

Figure 6. Representative engineering stress vs strain curves for *d*CPEPC copolymers.

Table 4. Ultimate Properties for Drawn CEC, CPC, and CPEPC Block Copolymers

sample	E (MPa)	ϵ_{fail}	σ_{fail} (MPa)
*d*CEC	280 ± 41	0.86 ± 0.18	92 ± 21
*d*CPEPC-70	111 ± 17	1.22 ± 0.22	75 ± 10
*d*CPEPC-50	64 ± 8	2.12 ± 0.17	59 ± 8
*d*CPEPC-30	31 ± 3	3.38 ± 0.34	47 ± 6
*d*CPC	18 ± 3	5.04 ± 0.17	32 ± 2

Representative engineering stress−strain curves for the cold drawn block copolymers are shown in Figure 6, and results averaged over multiple samples are enumerated in Table 4. As ξ increases, the elastic modulus and the rate of strain hardening of the drawn samples increase. The failure stress σ_{fail} also increases monotonically with a concomitant decrease in the failure strain ϵ_{fail}; however, these values represent lower bounds for the ultimate tensile strength since most samples break in close proximity to the grips. A linear correlation of σ_{fail} as a function of ξ is apparent in Figure 7a, while deviations from linearity are observed in the analogous plot of ϵ_{fail} (Figure 7b). The elastic moduli of these samples also increase nonlinearly with respect to ξ (Figure 7c).

Cyclic elasticity tests were performed on cold-drawn CEC, CPEPC-50, and CPC in which samples were cycled 15 times to 60% of their average breaking strain. Notably, none of the samples failed during these tensile−compression cycles. The cyclic tensile behavior asymptotically approaches a limiting

mechanical response curve shown in Figure 8. A decrease in the maximum stress after the first cycle is observed for all samples. Known as the Mullins effect or stress softening,[37] this effect is observed for many elastomers upon cyclic loading. While stress softening is most pronounced when $\xi = 0$, the recoverability for these materials is much greater. The enhanced recoverability of CPC as compared to CPEPC parallels the higher degree of elastic recovery documented for SPS compared to SPE.[26]

Discussion

Phase Behavior and Morphology. On the basis of SAXS and rheological analyses, we conclude that all of the C/P/E materials in Table 1 adopt a lamellar microphase separated structure in the melt. The phase behavior of these block copolymers depends sensitively on the molecular weight. Bates and co-workers[16,38,39] quantitatively determined that the sequence of temperature-dependent interaction parameters is

$$\chi_{CE}(T) > \chi_{CP}(T) \gg \chi_{EP}(T)$$

Since the molecular weights of the E and the P blocks are significantly lower than those required for melt microphase separation of the PEP segment (<145 kDa total at 114 °C, above $T_{m,E}$),[32] each CPEPC adopts a two domain lamellar structure comprised of alternating stacks of C and mixed E/P domains in the melt. The mixing of the E and P segments suggests that a single interaction parameter $\chi_{C-E/P}$ may account for the phase behavior of these melts due to the small magnitude of χ_{EP}. If we assume that this interaction parameter exhibits the conventional temperature dependence $\chi_{C-E/P} = (A/T) + B$ and that $(\chi N)_{ODT}$ is constant at fixed composition, N/T_{ODT} should be nearly constant. Evaluation of N/T_{ODT} for CPEPC-50 and CPEPC-50b shows quantitative agreement within 6%, neglecting slight compositional variations. Therefore, the strong molecular weight (M_n) dependence of T_{ODT} is captured by this simple argument.

Since the location of T_{ODT} dictates the processability of microphase-separated block copolymers, we compared our experimentally observed T_{ODT} data with theoretically predicted spinodal temperatures (T_s) from the random phase approximation (RPA)[40,41] to evaluate the efficacy of this tool in the design of new materials. While comparisons of theoretically predicted T_s to experimental T_{ODT} are not rigorously founded, experimental data have been successfully correlated with RPA predictions for various triblock copolymers comprised of three monomers.[41] For each experimental composition, T_s was calculated from the generalized RPA for ABC triblock copolymers using experimentally determined temperature-dependent interaction parameters.[16,38,39] The RPA predicts T_s in absolute temperature within 15% of the measured T_{ODT} for all of the polymers listed in Table 1, except CEPEC-50 (Table 1). In spite of expected deviations between T_s and T_{ODT} and the caveat that the RPA neglects the important effects of composition fluctuations,[38] we find remarkable agreement between this theory and our experimental data. The failure of the RPA to account for the phase behavior of CEPEC-50 suggests that these neglected effects are important. The behavior of the isomeric CPEPC and CEPEC can be qualitatively rationalized from the magnitudes of the relevant interaction parameters. Covalent linkages in CPEPC specify C−P interfaces that screen the C blocks from high-energy contacts with the E block, thus stabilizing the ordered state; in the disordered state, unfavorable C−E interactions occur. The CEPEC sequence instead forces contact between the C and E segments, thus favoring the disordered state in which high-energy C−E contacts are diluted with lower energy C−P monomer contacts.

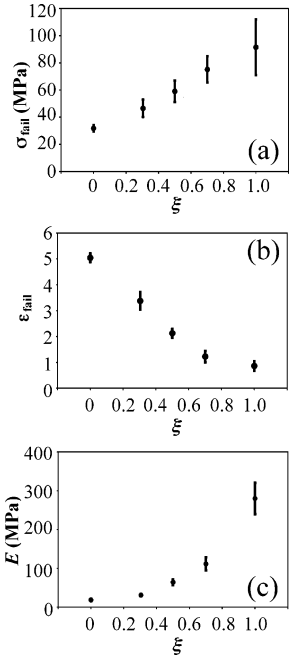

Figure 7. Plots of (a) σ_{fail} vs ξ, and (b) ϵ_{fail} vs ξ and (c) the elastic modulus E *vs* ξ for *d*CPEPC.

Two distinct modes of segregation hierarchically microphase separate the CPEPC pentablock copolymers: (i) segregation due to chemical incompatibility and (ii) E block crystallization-induced segregation. Since T_{ODT} is higher than the glass transition temperature of the C blocks ($T_{g,C} \sim 125$ °C) and the crystallization temperature of the E blocks ($T_{c,E} \sim 50-60$ °C), cooling from the disordered state initially yields melt microphase-separated two domain lamellae due to chemical incompatibility. Decreasing the temperature cements the lamellar structure by vitrification of the C blocks, while the E and P blocks remain fluid. Finally, the mixed E/P microdomains segregate by crystallization of the E block, which ejects the amorphous P ($T_{g,P} \sim -60$ °C). The reduced melting temperature of the geometrically confined E crystallites within the lamellar microdomains as compared to E homopolymer ($T_{m,E} \sim 110$ °C) concurs with prior observations by Weimann et al.[34] The increase in $T_{m,E}$ with ξ reflects an increase in the E crystal thickness,[42,43] which may derive from higher concentrations of E in the mixed E/P microdomain that promote increased interchain crystallization due to a lower degree of E/P compatibilization. The observed increase in X_c with decreasing ξ supports the notion that C−P contacts dominate the interface of the C and mixed E/P domains, such that the amorphous P block screens the hard C interface and provides increased mobility to the E chains, thus enabling more complete crystallization. A higher X_c probably lowers the entanglement density in the amorphous E segments, thus influencing the mechanical properties.[44]

Mechanical Properties of the Polydomain Samples. Comparison of the mechanical properties of CPE-50 and CPEPC-50 underscores the need to anchor the ends of the center PEP segment with glassy C to obtain tough materials (Figure 3). The pentablock architecture entraps entanglements between the glassy end blocks and prevents them from unraveling, thus providing an entangled network that exhibits enhanced toughness.[45−47] This molecular architecture effect on mechanical properties parallels the improved toughness of SBS relative to

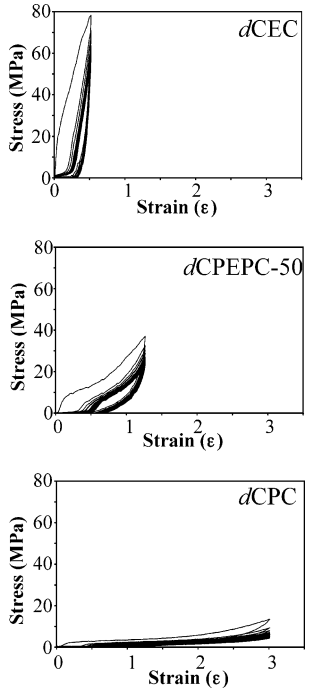

Figure 8. Engineering stress vs strain curves for *d*CPEPC in 15 cyclic tensile−compression tests.

SB[45] and CEC relative to CE.[22] The significantly larger elastic modulus of CPE-50 relative to CPEPC-50 is attributed to the presence of thicker, high modulus E crystals, evidenced by the higher melting temperature of CPE-50.

Trends in the elastic modulus (E) and yield stress (σ_{yield}) in the CPEPC polymer series provide some insights into the roles of the glassy, elastomeric, and semicrystalline blocks in dictating mechanical response. For CPC, the elastic modulus E and σ_{yield} reflect baseline values required to distort and break up the glassy C portions of the polydomain lamellar structure. Since f_C and M_n for the C blocks are nearly invariant across the series, the monotonic increases in E and σ_{yield} with ξ result from replacing the low-modulus P with more rigid semicrystalline E. This behavior is analogous to the expected result of adding a rigid filler to an elastomeric material. The increase in σ_{yield} with ξ may be explained by the increasing thickness of the E crystallites in these materials, given that the dependence of the yield stress of E homopolymer on crystallite size is well documented.[48] The nonlinear increases in E and σ_{yield} with ξ may also reflect the nontrivial mechanical coupling of polymer chains through interchain cocrystallization of the E segments[49] and changes in the entanglement density.[44]

Ultimate properties such as the stress σ_{fail} and strain ϵ_{fail} at break also exhibit revealing trends. With decreasing ξ, ϵ_{fail} increases monotonically since the larger P blocks confer improved ductility; the limiting behavior of CPC is reminiscent of that of SBS and SIS. This increased ductility delays the onset of the activation of defects and the failure of the glassy C domains, thus allowing the material to achieve increased stress levels at increased strains. Surprisingly, CPEPC-70 exhibits superior ductility compared to CEC with a significant increase in ultimate strength (Table 2). Assuming an affine uniaxial deformation, we find that the true stress at break ($\sigma_{fail,\ true} = (1 + \epsilon_{fail})\sigma_{fail}$) systematically decreases from 222 MPa for CPC to 107 MPa for CEC. This implies that incorporation of semicrystalline E lowers the failure stresses of these materials akin to the effects of adding high modulus, brittle fillers to an elastomer. Given the slight decrease in the overall E crystallinity and

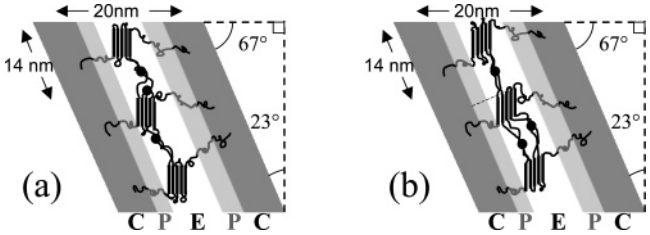

Figure 9. An illustration of two possible microstructures of *d*CPEPC-50 deduced from SAXS and WAXS data in Figure 5 in which (a) the E crystal fold surfaces are perpendicular to the draw direction and (b) the E crystal fold surfaces are perpendicular to the microphase-separated lamellar interfaces.

increasing overall M_n as $\xi \rightarrow 0$, the amorphous entanglement density in the PEP segment may increase. This increased entanglement density of the amorphous segments probably contributes significantly to the observed increase in strength.[44]

Effects of Cold Drawing. Cold drawing substantially alters the polydomain structure of the lamellar CPEPC materials, producing samples that exhibit high values of σ_{fail} (Table 4). SAXS reveals that drawing deforms the randomly oriented lamellae, resulting in elliptical scattering patterns (Figure 4). This elliptical scattering pattern signifies an anisotropic deformation of the sample: domains having lamellae normal to the strain direction are either dilated or reoriented giving rise to low q scattering, whereas domains with lamellae parallel to drawing direction contract to yield high q scattering. The ratio of $|\mathbf{q}^*|$ along the strain axis (meridian) for drawn samples to that of the undeformed samples matches the observed permanent set; however, the intensity along this direction is quite low. In previous studies of lamellar SBS triblocks under tension,[2,4,9] similar SAXS patterns were ascribed to reorientation or destruction of ordered lamellar interfaces perpendicular to the strain axis.[3] The appearance of two pairs of intense spots located ±23° from the equator for *d*CPEPC-50 suggests that drawing preferentially tilts the lamellar grains such that the flat interfaces are oriented ±23° from the drawing direction (Figure 9). Simple grain rotation in polydomain samples under tension is restricted, since chains that span grain boundaries in the bulk sample will inhibit such action. The fact that the four intense peaks appear at $|\mathbf{q}| = 0.031$ Å^{-1} equal to that of the undrawn CPEPC-50 implies that grain reorientation involves a combination of dilation and shear along the lamellar interfaces in order to maintain a constant domain spacing. Cohen et al. previously reported a similar type of "affine rotation", a combination of dilation and shear deformation, in macroscopically oriented SBS triblock copolymer samples.[9] The low degree of pronounced off-axis scattering in the *d*CPC may be due to the small permanent set, which translates into indistinguishable scattering intensity along the broken ellipse with small eccentricity (Figure 4). The nearly contiguous ellipse in *d*CEC indicates that the lamellae perpendicular to the drawing axis deform by dilating. The mechanical properties of CPEPC and *d*CPEPC thus represent a complex average of the collective mechanical response of grains having different orientations relative to the strain axis.

Cold drawing also changes the preferred orientation of the E crystals within the deformed lamellar structure. WAXS analysis of *d*CPEPC-50 reveals the alignment of the E crystal stems along the drawing direction (Figure 5b). The correlation of increased permanent set with ξ mirrors the larger amount of crystalline E that is plastically deformed during drawing. SAXS patterns of all of the *d*CPEPC exhibit four broad scattering maxima at $d \sim$ 14 nm, which are associated with the intercrystal correlation length in the E domains (Figure 4 and 5a). The location of these

scattering maxima ±23° from the meridian in *d*CPEPC-50 implies that the direction of this correlation length coincides with the aligned lamellar interfaces therein (Figures 5d and 9). The shear deformation of the lamellar domains by cold drawing probably causes a combination of reorientation of the E crystals nested within the amorphous P block and shear-induced melting and recrystallization of the E blocks to furnish the observed morphology.[48,50] The apparent increase in intercrystal scattering intensity reflects the macroscopic orientation of the E crystallites along the drawing direction with the preferred intercrystal correlation length coincident with the aligned lamellar interfaces, in contrast to the broad intercrystal scattering observed from the isotropic crystallite orientation in the undrawn materials. On the basis of the above scattering analyses, we formulate two possible microstructural models depicted in Figure 9 for *d*CPEPC-50 that are consistent with the data presented above. While many studies of polyethylene crystallization conclude that the E crystal stems are arranged perpendicular to the fold surface as shown in Figure 9a, E crystals in which the crystal fold surface is at a steep angle relative to the chain axes (Figure 9b) have also been observed in polyethylene prepared by solution crystallization and melt-drawing.[51]

The tensile properties of *d*CPEPC exhibit trends that may be useful in designing polyolefin materials with intermediate properties. For *d*CPEPC, σ_{fail} increases nearly linearly with ξ, while ϵ_{fail} decreases nearly linearly (Figure 7). The elastic modulus and rate of strain hardening for these samples also increase with increasing ξ (Figures 6 and 7c). The exchange of low-modulus P for semicrystalline E having lower extensibility may account for this observation; however, the overall crystalline weight fraction of each CPEPC is ~8−10%. Recent tensile calorimetry experiments demonstrate the nontrivial role of strain-induced crystallization on the strain hardening response of styrenic block copolymers with semicrystalline segments.[52] In the *d*CPEPC materials, orientation of the E crystals as well as substantial amounts of the amorphous "interphase"[53] could enhance the propensity for strain-induced crystallization. Alternatively, the variable tensile properties of the *d*CPEPC series may simply stem from changes in the entanglement density of the PEP segment, which depends sensitively upon the crystallinity X_c and the processing history.[44] The relative roles of strain-induced crystallization and changes in entanglement density remain unknown and warrant further investigation.

Since the mechanical strength of block copolymers is thought to derive from trapped entanglements, quantitative theories accounting for the tensile properties of these materials have been developed. By modeling an amorphous styrenic triblock copolymer as an amorphous rubber modified with a glassy filler, Holden et al. derived a correlation between the elastic modulus of a block copolymer and $(1/M_c)$, where M_c is the molecular weight between chain entanglements.[10] Unfortunately, this model does not account for the ultimate mechanical properties of these materials. Tong and Jerôme[54] subsequently proffered a model in which the ultimate strength of a triblock elastomer is related to $(1/M_e)$, where M_e is the entanglement molecular weight of the rubbery homopolymer segment. Scarce experimental data on the exact number of amorphous entanglements of a block copolymer coupled with the presence of a semicrystalline block, which exhibits inherently plastic rather than elastic behavior, prevent application of either of these models to the CPEPC materials.

The low degree of stress softening of the CPEPC polymers in cyclic loading experiments accentuates their distinct mechanical response from that of traditional styrenic thermoplastic elastomers. Cyclic loading of triblock thermoplastic elastomers destroys the integrity of the glassy component, leading to huge reductions in the maximum stress achieved akin to that observed for CPC (Figure 8). Alternative mechanisms for accommodating stress in the E-containing materials, such as strain-induced crystallization or simple load bearing by the E crystals, must play an important role in lowering the degree of stress softening and in delaying ultimate compromise of the mechanical integrity of the glassy block.

Conclusion

The phase behavior, microstructure, and tensile characteristics of lamellae-forming CPEPC block copolymers with $w_C \sim 0.4$ and $0 \leq \xi \leq 1$ were investigated in order to elucidate the mechanical consequences of incorporating a semicrystalline domain into a traditional "hard−soft" thermoplastic elastomer. Since the processability of these materials depends on the location of the order−disorder transition temperature, we examined the effects of molecular weight and block sequence on the melt-phase behavior of these materials. On the basis of this analysis and the thermal characteristics of the constituent blocks, we conclude that these materials undergo melt-microphase separation into a lamellar structure that templates subsequent crystallization of the E blocks. These polyolefins exhibit a wide array of mechanical responses, which depend on the relative volume fractions of the elastomeric and semicrystalline blocks. The elastic modulus and yield stress increase with ξ, while the ultimate strength and the elongation at break decrease. Processing these polymers by cold drawing yields samples with significantly improved tensile properties, the origins of which were probed at the microstructural level using SAXS and WAXS. Cold drawing causes a shear deformation that preferentially orients the lamellar structure and the polyethylene crystallites therein. Cold drawn CPEPC materials exhibit a low degree of stress softening in cyclic recovery tests, as compared to the completely amorphous CPC. Studies that examine the deformation behaviors of "single-grain" CPEPC samples are in progress to further understand the contributions of the glassy, elastomeric, and semicrystalline block on the overall mechanical response.

Acknowledgment. The authors gratefully acknowledge financial support from Medtronic Corp., the Department of Energy through a subcontract to UT-Battelle (No. 4000041622), and the National Science Foundation Materials Research Science and Engineering Center (NSF-MRSEC) at the University of Minnesota (NSF DMR-0212302). This research made extensive use of NSF-MRSEC supported characterization facilities at the University of Minnesota. Portions of this work were performed at the DuPont-Northwestern-Dow Collaborative Access Team (DND-CAT) Synchrotron Research Center located at Sector 5 of the Advanced Photon Source (Argonne, IL). DND-CAT is supported by the E.I. DuPont de Nemours & Co., the Dow Chemical Co., and the NSF (DMR-9304725). Use of the Advanced Photon Source was supported by the U.S. Department of Energy, Office of Basic Energy Sciences, under Contract No. W-31-109-Eng-38. The authors also thank Yonathan Thio, Chong Min Koo, and Alhad Phatak for enlightening discussions and Eric Cochran for assistance with RPA calculations.

References and Notes

(1) Holden, G., Legge, N. R., Quirk, P. R., Schroeder, H. E., Eds. *Thermoplastic Elastomers*, 2nd ed.; Hanser Publishers: New York, 1996.

(2) Séguéla, R.; Prud'homme, J. *Macromolecules* **1981**, *14*, 197−202.

(3) Pakula, T.; Saijo, K.; Kawai, H.; Hashimoto, T. *Macromolecules* **1985**, *18*, 1294−1302.
(4) Fujimura, M.; Hashimoto, T.; Kawai, H. *Rubber Chem. Technol.* **1978**, *51*, 215.
(5) Honeker, C. C.; Thomas, E. L. *Chem. Mater.* **1996**, *8*, 1702−1714.
(6) Kawai, H.; Hashimoto, T.; Miyoshi, K.; Uno, H.; Fujimura, M. *J. Macromol. Sci., Phys.* **1980**, *B17*, 427−472.
(7) Morton, M.; McGrath, J. E.; Juliano, P. C. *J. Polym. Sci., Part C* **1969**, *26*, 99−115.
(8) Cohen, Y.; Thomas, E. L. *Macromolecules* **2003**, *36*, 5265−5270.
(9) Cohen, Y.; Albalak, R. J.; Dair, B. J.; Capel, M. S.; Thomas, E. L. *Macromolecules* **2000**, *33*, 6502−6516.
(10) Holden, G.; Bishop, E. T.; Legge, N. R. *J. Polym. Sci., Part C* **1969**, *26*, 37−57.
(11) Bates, F. S.; Fredrickson, G. H.; Hucul, D. A.; Hahn, S. F. *AIChE J.* **2001**, *47*, 762−765.
(12) Hucul, D. A.; Hahn, S. F. *Adv. Mater.* **2000**, *12*, 1855−1858.
(13) Zhao, J.; Hahn, S. F.; Hucul, D. A.; Meunier, D. M. *Macromolecules* **2001**, *34*, 1737−1741.
(14) Patel, R. M.; Hahn, S. F.; Esneault, C.; Bensason, S. *Adv. Mater.* **2000**, *12*, 1813−1817.
(15) Vigild, M. E.; Chu, C.; Sugiyama, M.; Chaffin, K.; Bates, F. S. *Macromolecules* **2001**, *34*, 951−964.
(16) Cochran, E. W.; Bates, F. S. *Macromolecules* **2002**, *35*, 7368−7374.
(17) Ryu, C. Y.; Ruokolainen, J.; Fredrickson, G. H.; Kramer, E. J. *Macromolecules* **2002**, *35*, 2157−2166.
(18) Ruokolainen, J.; Fredrickson, G. H.; Kramer, E. J.; Ryu, C. Y.; Hahn, S. F.; Magonov, S. N. *Macromolecules* **2002**, *35*, 9391−9402.
(19) Hermel, T. J.; Wu, L.; Hahn, S. F.; Lodge, T. P.; Bates, F. S. *Macromolecules* **2002**, *35*, 4685−4689.
(20) Hermel, T. J.; Hahn, S. F.; Chaffin, K.; Gerberich, W. W.; Bates, F. S. *Macromolecules* **2003**, *36*, 2190−2193.
(21) Mori, Y.; Lim, L. S.; Bates, F. S. *Macromolecules* **2003**, *36*, 9879−9888.
(22) Lim, L. S.; Harada, T.; Hillmyer, M. A.; Bates, F. S. *Macromolecules* **2004**, *37*, 5847−5850.
(23) Phatak, A.; Macosko, C. W.; Bates, F. S.; Hahn, S. F. *J. Rheol.* **2005**, *49*, 197−213.
(24) Balsamo, V.; von Gyldenfeldt, F.; Stadler, R. *Macromolecules* **1999**, *32*, 1226−1232.
(25) Heuschen, J.; Vion, J. M.; Jerome, R.; Teyssie, P. *Macromolecules* **1989**, *22*.
(26) Schmalz, H.; Boker, A.; Lange, R.; Krausch, G.; Abetz, V. *Macromolecules* **2001**, *34*, 8720−8729.
(27) Ndoni, S.; Papadakis, C. M.; Bates, F. S.; Almdal, K. *Rev. Sci. Instrum.* **1995**, *66*, 1090−5.
(28) Brandrup, J.; Immergut, E. H. *Polymer Handbook*, 3rd ed.; John Wiley & Sons: New York, 1989.
(29) Fetters, L. J.; Lohse, D. J.; Richter, D.; Witten, T. A.; Zirkel, A. *Macromolecules* **1994**, *27*, 4639−47.
(30) Rosedale, J. H.; Bates, F. S. *Macromolecules* **1990**, *23*, 2329−38.
(31) Gehlsen, M. D.; Almdal, K.; Bates, F. S. *Macromolecules* **1992**, *25*, 939−43.
(32) Koo, C. M.; Wu, L.; Lim, L. S.; Mahanthappa, M. K.; Hillmyer, M. A.; Bates, F. S. *Macromolecules* **2005**, *38*, 6090−8.
(33) Bates, F. S. *Macromolecules* **1985**, *18*, 525−8.
(34) Weimann, P. A.; Hajduk, D. A.; Chu, C.; Chaffin, K.; Brodil, J. C.; Bates, F. S. *J. Polym. Sci., Part B: Polym. Phys.* **1999**, *37*, 2053−2068.
(35) Koo, C. M.; Hillmyer, M. A.; Bates, F. S. *Macromolecules* **2006**, *39*, 667−677.
(36) Uehara, H.; Nakae, M.; Kanamoto, T.; Zachariades, A. E.; Porter, R. S. *Macromolecules* **1999**, *32*, 2761−2769.
(37) Trabelsi, S.; Albouy, P.-A.; Rault, J. *Macromolecules* **2003**, *36*, 9093−9099.
(38) Rosedale, J. H.; Bates, F. S.; Almdal, K.; Mortensen, K.; Wignall, G. D. *Macromolecules* **1995**, *28*, 1429−43.
(39) Maurer, W. W.; Bates, F. S.; Lodge, T. P.; Almdal, K.; Mortensen, K.; Fredrickson, G. H. *J. Chem. Phys.* **1998**, *108*, 2989−3000.
(40) Leibler, L. *Macromolecules* **1980**, *13*, 1602−17.
(41) Cochran, E. W.; Morse, D. C.; Bates, F. S. *Macromolecules* **2003**, *36*, 782−92.
(42) Bassett, D. C. *Principles of Polymer Morphology*; Cambridge University Press: New York, 1981; pp 146−166.
(43) Mandelkern, L.; Stack, G. M. *Macromolecules* **1984**, *17*, 871−8.
(44) Schrauwen, B. A. G.; Janssen, R. P. M.; Govaert, L. E.; Meijer, H. E. H. *Macromolecules* **2004**, *37*, 6069−78.
(45) Matsuo, M.; Ueno, T.; Horino, H.; Chujyo, S.; Asai, H. *Polymer* **1968**, *9*, 425−36.
(46) Beecher, J. F.; Marker, L.; Bradford, R. D.; Aggarwal, S. L. *Polym. Prepr.* **1969**, *8*, 1532.
(47) Holden, G.; Legge, N. R. In *Thermoplastic Elastomers*, 2nd ed.; Holden, G., Legge, N. R., Quirk, P. R., Schroeder, H. E., Eds.; Hanser Publishers: New York, 1996; pp 47−70.
(48) Galeski, A. *Prog. Polym. Sci.* **2003**, *28*, 1643−99.
(49) Séguéla, R. *J. Polym. Sci., Part B: Polym. Phys.* **2005**, *43*, 1729−48.
(50) Seguela, R. *J. Macromol. Sci., Polym. Rev.* **2005**, *C45*, 263−87.
(51) Schultz, J. *Polymer Materials Science*; Prentice Hall: Englewood Cliffs, NJ, 1974; pp 30−39.
(52) Indukuri, K. K.; Lesser, A. J. *Polymer* **2005**, *46*, 7218−7229.
(53) Mowery, D. M.; Harris, D. J.; Schmidt-Rohr, K. *Macromolecules* **2006**, *39*, 2856−65.
(54) Tong, J.-D.; Jerome, R. *Macromolecules* **2000**, *33*, 1479−81.

MA0617421